Reaction Kinetics of Nitric Oxide on Size-Selected Silver Cluster Cations

Arakawa, Masashi
Department of Chemistry, Faculty of Science, Kyushu University

Horioka, Masataka
Department of Chemistry, Faculty of Science, Kyushu University

Minamikawa, Kento
Department of Chemistry, Faculty of Science, Kyushu University

Kawano, Tomoki
Department of Chemistry, Faculty of Science, Kyushu University

他

出版情報：The Journal of Physical Chemistry C. 124 (49), pp.26881-26888, 2020-11-27. American Chemical Society (ACS)
バージョン：

Reaction Kinetics of Nitric Oxide on Size-Selected Silver Cluster Cations

Masashi Arakawa, Masataka Horioka, Kento Minamikawa, Tomoki Kawano, and Akira Terasaki**

Department of Chemistry, Faculty of Science, Kyushu University, 744 Motooka, Nishi-ku, Fukuoka 819-0395, Japan

ABSTRACT

We report reaction of gas-phase free silver cluster cations, Ag_n^+ (n = 3–18), with nitric oxide molecules studied by kinetics measurement using an ion trap. $Ag_nO(NO_2)_{m-1}^+$ and $Ag_n(NO_2)_m^+$ are observed as major products after multiple reactions. The reaction pathway to form these product ions is identified by fitting the data to rate equations for $n \leq 15$ except for inert n = 3 and 5. Two different reaction mechanisms are found for formation of these products depending on cluster size; pseudo-first-order rate constants of each step of elementary reactions are obtained. First, as found for n = 4, 6, and 9, Ag_nO^+ is formed by reaction with two NO molecules followed by release of neutral N_2O. Further reaction of Ag_nO^+ with another NO molecule produces $Ag_nNO_2^+$. $Ag_n(NO_2)_m^+$ ($m \geq 1$) is thus successively formed via the intermediate, $Ag_nO(NO_2)_{m-1}^+$. This is analogous to the reaction of NO on silver surfaces to produce NO_2. Second, both $Ag_nNO_2^+$ and Ag_nO^+ are formed concurrently as found for n = 7, 8, 10, 11, 12, and 15; Ag_nO^+ does not act as an intermediate for $Ag_nNO_2^+$. $Ag_nO(NO_2)_{m-1}^+$ and $Ag_n(NO_2)_m^+$ ($m \geq 2$) are formed by successive addition of NO_2 to Ag_nO^+ and $Ag_nNO_2^+$, respectively. It is speculated that the successive addition of NO_2 proceeds via disproportionation, i.e., three NO molecules are converted to NO_2 and N_2O. The reaction pathways of n = 13 and 14 are explained equally well by the two mechanisms. The overall reaction coefficients exhibit odd−even alternation; the higher reactivity for even n is due to an odd number of valence electrons.

1. INTRODUCTION

Nitric oxide, NO, is a radical of great importance, as is known as one of the signaling molecules involved in various physiological processes[1,2] and as a ligand forming nitrosyl compound with almost all the transition metals. On the other hand, NO is one of the toxic gases generated during combustion processes in automobile engines and thermal power stations, which causes environmental issues such as photochemical smog and acid rain. In this context, catalytic reactions for removal and reduction of NO has been studied.[3,4] Among these studies, catalytic reduction of NO by hydrocarbons on alumina supported silver surface (Ag/Al_2O_3) is one of the most effective and promising reactions.[5–10]

NO molecules on a Ag surface have been studied experimentally[11–26] and theoretically[26–30] to understand adsorption and subsequent reaction of NO molecules. Two NO molecules are known to produce N_2O and O, where the reaction mechanism has been the subject of debate.[12,13,15–17,19–21,23,24–26,30] A study examining isotopic distribution of the reaction products from $^{14}N^{16}O$ and $^{15}N^{18}O$ on a Ag(111) surface revealed that N_2O was formed via $(NO)_2$ dimer as an intermediate.[19] The formation of the dimer was supported by photoelectron spectroscopy,[13,23] thermal desorption spectroscopy,[15] X-ray absorption near edge structure,[20] reflection-absorption infrared spectroscopy,[20,21] scanning tunneling microscopy,[26] and theoretical calculations.[30] A N_2O molecule and an O atom are formed from the dimer at 75–100 K, which is followed by a further reaction of the O atom with another NO molecule to produce nitrogen dioxide, NO_2.[19]

Metal clusters consisting of a finite number of atoms have been attracting much attention as model systems of heterogeneous catalysts, because they provide molecular-level insights into metal-mediated catalytic reactions.[31] Theoretical studies demonstrated

formation of $(NO)_2$ dimer on Ag clusters[32] and subsequent reduction to N_2O,[33] although energy barrier for dissociation of a single NO molecule is reported to be high.[34] An adsorption site of NO was also reported,[35–38] where the molecular orbital shape of the frontier orbitals was found to play a key role in site selectivity.[37,38] Theoretical calculations also revealed that Ag clusters with odd numbers of electrons exhibit adsorption energies higher than those with even electrons.[39,40]

In addition to these theoretical studies, reaction of Ag clusters with NO molecules has been investigated experimentally.[41–43] Kinetic measurement was performed for gas-phase anionic clusters, Ag_n^-; fragmentation of the clusters was the major reaction channel for n = 1–4, whereas Ag_5^- produced $Ag_5N_xO_y^-$ ($x < y$).[41] Reaction of NO with O_2 on Ag_6^+ supported on zeolite was reported using EPR spectroscopy.[42] More recently, the experiment was extended to a broader size range, where reaction of $Ag_n^\pm$ (n = 7–69) with NO in the gas phase was examined to report formation of $Ag_nNO^\pm$ and $Ag_n(NO)_2^\pm$ as a major products along with $Ag_nO^\pm$ and $Ag_nNO_2^\pm$ for several small sizes;[43] formation of $Ag_nO^\pm$ implies release of N_2O.

As for other transition-metal clusters, gas-phase reaction with NO has been reported for Co_n^+,[44–48] Ni_n^-,[49] $Cu_n^{\pm/0}$,[50,51] $Nb_n^\pm$,[52] $Rh_n^\pm$,[53,54] V_nO_m,[55] Ta_nO_m,[55] $Cu_nO_m^\pm$,[51,56] $Ce_nO_m^+$,[57] and Cu_nAl^+.[58] Dissociative adsorption of NO on cobalt cluster cations, Co_n^+,[44,46] is followed by release of N_2 to produce O_2 adducts.[47,48] Sequential adsorption of NO and release of N_2 have also been reported for $Rh_n^\pm$.[53,54] NO molecules adsorbed on $Cu_n^{\pm/0}$ do not exhibit reaction between them,[50,51] whereas their reactivity is altered by oxidation or by doping of Al; oxidation of NO to NO_2 is reported for $Cu_nO_m^+$,[51] while release of N_2 has been observed for $Cu_nO_2^-$ and Cu_nAl^+.[56,58] It is also reported that NO is reduced to N_2O by Cu nanoclusters on an Al_2O_3 film.[59] These reactions show that Cu

opens various reaction channels when it is combined with other elements. For Ni_n^- and Nb_n^-, on the other hand, production of NO_2^- and NO_3^- via electron transfer from the cluster was observed as well as release of N_2 forming oxidized cluster anions.[49,52] For Nb_n^+, formation of $Nb_nN_2O^+$ and $Nb_nNO_2^+$ are observed.[52] As for oxide clusters of V, Ta, and Ce, NO adsorption is the only reaction channel for $V_nO_m^+$ and $Ta_nO_m^+$,[55] whereas NO is oxidized to NO_2 by $Ce_nO_m^+$ forming $Ce_nO_{m-1}^+$.[57] NO thus shows a rich variety of reactions depending on the catalysts. In addition to these reaction experiments, IR multiphoton dissociation spectroscopy was reported for Au_nNO^+ and Rh_nTaNO^+.[60,61] Odd–even oscillation was reported for the NO stretching frequency of Au_nNO^+.[60] Geometric and electronic structures of NO adducts, $Fe_nNO^{\pm}$,[62] $Rh_nNO^{\pm/0}$,[63] Pd_nNO^+,[64] and $Au_nNO^{\pm/0}$,[65,66] were optimized by DFT calculations.

As the above-mentioned studies of NO reactions on clusters have been focusing on the reaction products and their structures, kinetics information is still lacking. In the present study, we perform reaction kinetics measurement on size-selected silver cluster cations, Ag_n^+ (n = 3–18), by employing an ion trap. We report reaction pathways and rates of each step by analyzing time-dependent changes in the reactant and product ion signals.

2. EXPERIMENTAL PROCEDURES

The experimental setup used for reaction kinetics measurement has been described in detail elsewhere.[67] Briefly, Ag_n^+ (n = 3–18) was generated by a magnetron-sputter cluster-ion source, where sputtering of a silver plate (Toshima Manufacturing Co., Ltd., 99.99%) was followed by aggregation of sputtered atoms and ions through collisions with a buffer helium gas (99.99995%) cooled by liquid nitrogen. After thermalization by

collisions with a helium gas at liquid-nitrogen temperature, the cluster cations were mass selected by a quadrupole mass filter (MAX-4000, Extrel CMS, LLC). The size-selected reactant cations were guided by radio-frequency (rf) octopole ion guides and quadrupole deflectors, and were introduced into a 30-cm-long linear quadrupole ion trap, which was placed in a reaction gas cell at room temperature filled with buffer helium of 0.3 Pa and pressure-controlled reactant nitric oxide. The partial pressure of reactant nitric oxide, P_{NO}, was adjusted in the range between 3×10^{-3} and 3×10^{-2} Pa depending on the magnitude of reactivity so that the time constant of the reaction comes into the time window of the measurement. The pressures of He and NO gases were measured by a residual gas analyzer (RGA100, Stanford Research Systems, Inc.) outside the gas cell, which were converted to the pressure inside the gas cell as reported previously[68] by referring to the reaction cross sections of Co_n^+ with O_2.[69] A care was taken to prevent NO from reacting with a trace amount of residual O_2 or H_2O in the gas line and the gas cell, which causes conversion of NO to NO_2. It was confirmed that the partial pressure of NO_2 was less than 0.1% of that of NO as observed by the RGA.

After the ion trap was loaded with reactant cluster ions for 50–200 ms, the ions were stored for a variable time, t, for reaction. Product ions were extracted from the ion trap for analysis by a reflectron time-of-flight (TOF) mass spectrometer.[70] The TOF mass spectra were accumulated for 1,000 cycles of trap and detection. The yields of reactant and product ions were measured as a function of storage time t to evaluate reaction rate constants.

3. RESULTS AND DISCUSSION

3.1. Reaction Products. Figure 1 shows mass spectra of product ions upon reaction of Ag_n^+ with NO molecules for n = 3–18. The partial pressure of NO, P_{NO}, and storage time, t, are shown in each panel. Ag_3^+ and Ag_5^+ were exceptionally inert with no reaction products observed. Ag_4^+ and Ag_6^+ are similar in that a dissociated product ion, Ag_{n-1}^+, was dominant along with small amounts of Ag_nO^+ and $Ag_nNO_2^+$; formation of Ag_{n-1}^+ implies release of neutral AgNO after NO adsorption. Note that the dissociation channel to Ag_{n-1}^+ was also observed for Ag_{10}^+ but for no other sizes. As for sizes with $n \geq 7$, NO_2 adducts, $Ag_n(NO_2)_m^+$, were observed as major reaction products; the mass spectra exhibiting product peaks separated by a NO_2 unit, as observed clearly for $n \geq 11$, suggest that molecular NO_2 is formed on Ag_n^+ rather than that the N and O atoms are adsorbed dissociatively. Oxygen adducts, $Ag_nO(NO_2)_{m-1}^+$, were also observed as major product ions, e.g., Ag_6O^+, $Ag_7O(NO_2)^+$, Ag_8O^+, $Ag_{10}O^+$, $Ag_{11}O(NO_2)^+$, $Ag_{12}O(NO_2)_2^+$, $Ag_{13}O(NO_2)_3^+$, and $Ag_{14}O(NO_2)_2^+$, for n = 6–8, 10–14, respectively.

The present result is consistent with a previous study performed by a continuous flow reactor,[41] where Ag_nO^+, Ag_nNO^+, and $Ag_n(NO)_2^+$ are observed at 120 K as major reaction products along with a small amount of $Ag_nNO_2^+$. NO adducts, Ag_nNO^+, are observed probably due to the temperature lower than our present experiment performed at room temperature as well as a lower flow rate of the NO gas and a shorter reaction time. The present and the previous results of the cluster experiments are analogous to the reaction of NO on silver surfaces: adsorption of NO molecules on a silver surface produces N_2O and O atom at 75–100 K, and further reaction of the O atom with another NO molecule produces NO_2.[19] The present result with a significant amount of $Ag_n(NO_2)_m^+$ for $n \geq 7$ indicates that NO_2 molecules are formed successively during multiple collisions of Ag_n^+ with NO molecules.

3.2. Reaction Kinetics and Pathways. *3.2.1. Ag_6^+.* Figure 2 shows temporal evolution of ion signals of reactant and product ions in the reaction of Ag_6^+ with NO at $P_{NO} = 3 \times 10^{-3}$ Pa. Panels (a) and (b) show the same experimental data, but display kinetics analyses assuming different reaction pathways. The reactant, Ag_6^+, disappears exponentially with the storage time, while Ag_6O^+, $Ag_6NO_2^+$, and Ag_5^+, are produced accordingly. Note that reaction products are present even at 0.0 s, which are produced during ion loading prior to storage. The result shows that Ag_5^+ is produced as a major product, which exhibits an exponential rise to dominate the product ions eventually. As for the other two products, Ag_6O^+ appears to be produced first, being followed by formation of $Ag_6NO_2^+$.

The reaction pathway to form these product ions was identified by fitting the data to rate equations, where possible reaction pathways were examined to search for the most probable pathway. The present reactions take place in a pseudo-first-order process because the reaction cell enclosing the ion trap was filled with NO and He gases at constant partial pressures much higher than the corresponding density of the reactant ions, Ag_n^+. Curve fitting to the pseudo-first-order rate equations was performed for the following two reaction pathways (6A) and (6B):

$$\begin{array}{l} Ag_6^+ \xrightarrow{k_{6A,1}} Ag_6O^+ \xrightarrow{k_{6A,2}} Ag_6NO_2^+ \\ \quad\quad \downarrow_{k_{6A,3}} \\ \quad\quad Ag_5^+ \end{array} \qquad (6A)$$

$$d[Ag_6^+]/dt = -(k_{6A,1} + k_{6A,3})[Ag_6^+] \qquad (6A\text{-}1)$$

$$d[Ag_6O^+]/dt = k_{6A,1}[Ag_6^+] - k_{6A,2}[Ag_6O^+] \qquad (6A\text{-}2)$$

$$d[Ag_6NO_2^+]/dt = k_{6A,2}[Ag_6O^+] \qquad (6A\text{-}3)$$

$$d[Ag_5^+]/dt = k_{6A,3}[Ag_6^+] \qquad (6A\text{-}4)$$

$$\begin{array}{l} Ag_6^+ \xrightarrow{k_{6B,1}} Ag_6O^+ \xrightarrow{k_{6B,2}} Ag_5^+ \\ \quad\quad \searrow^{k_{6B,3}} \\ \quad\quad\quad Ag_6NO_2^+ \end{array} \qquad (6B)$$

$$d[Ag_6^+]/dt = -(k_{6B,1} + k_{6B,3})[Ag_6^+] \qquad (6B\text{-}1)$$

$$d[Ag_6O^+]/dt = k_{6B,1}[Ag_6^+] - k_{6B,2}[Ag_6O^+] \qquad (6B\text{-}2)$$

$$d[Ag_6NO_2^+]/dt = k_{6B,3}[Ag_6^+] \qquad (6B\text{-}3)$$

$$d[Ag_5^+]/dt = k_{6B,2}[Ag_6^+] \qquad (6B\text{-}4).$$

The pathway (6A) represents that $Ag_6NO_2^+$ is formed via Ag_6O^+ as an intermediate, while Ag_5^+ is produced concurrently with Ag_6O^+. On the other hand, (6B) assumes that Ag_6O^+ and $Ag_6NO_2^+$ are formed concurrently from Ag_6^+; Ag_5^+ is produced by release of neutral AgO from Ag_6O^+.

The results of the curve fitting are shown by solid lines in Figs. 2a and 2b for (6A) and (6B), respectively. The pseudo-first-order rate constants of each step of elementary reactions, $k_{6A,1}$, $k_{6A,2}$, and $k_{6A,3}$, are 0.23, 1.18, and 2.78 s^{-1}, respectively, in the pathway (6A), whereas $k_{6B,1}$, $k_{6B,2}$, and $k_{6B,3}$ are, 2.72, 17.71, and 0.23 s^{-1}, respectively, in (6B). The fitting to the pathway (6A) reproduces the temporal evolution of ion signals much better than (6B); in particular, ion signals of Ag_6O^+ fit very well to the curves obtained for (6A). Therefore, the reaction pathway is identified as (6A), i.e., $Ag_6NO_2^+$ is formed via intermediate Ag_6O^+. The intermediate might be produced from an ion–molecule complex, $Ag_6(NO)_2^+$, which is not discernible in the mass spectrum in Fig. 1d probably because of its short lifetime. The whole scinario is suggested as follows: Ag_6^+ reacts with two NO molecules to produce Ag_6O^+ and N_2O in the same manner as on a silver surface,[19] and subesquently Ag_6O^+ reacts further with another NO to form $Ag_6NO_2^+$.

3.2.2. Ag_8^+. Figure 3 shows a result of Ag_8^+ measured at $P_{NO} = 6 \times 10^{-3}$ Pa, where Ag_8O^+ and $Ag_8NO_2^+$ are the major product ions without any dissociation product, Ag_7^+. Panels (a) and (b) again show the same experimental, but display kinetics analyses assuming different reaction pathways. Ion signals of both Ag_8O^+ and $Ag_8NO_2^+$ increased exponentially with the storage time; $Ag_8NO_2^+$ dominated the product ions eventually.

The analysis of kinetics was carried out in the same way as in the case of Ag_6^+: curve fitting to the pseudo-first-order rate equations was performed for the following two reaction pathways (8A) and (8B):

$$Ag_8^+ \xrightarrow{k_{8A,1}} Ag_8O^+ \xrightarrow{k_{8A,2}} Ag_8NO_2^+ \qquad (8A)$$

$$d[Ag_8^+]/dt = -k_{8A,1}[Ag_8^+] \qquad (8A\text{-}1)$$

$$d[Ag_8O^+]/dt = k_{8A,1}[Ag_8^+] - k_{8A,2}[Ag_8O^+] \qquad (8A\text{-}2)$$

$$d[Ag_8NO_2^+]/dt = k_{8A,2}[Ag_8O^+] \qquad (8A\text{-}3)$$

$$Ag_8^+ \xrightarrow{k_{8B,1}} Ag_8O^+$$
$$\xrightarrow{k_{8B,2}} Ag_8NO_2^+ \qquad (8B)$$

$$d[Ag_8^+]/dt = -(k_{8B,1} + k_{8B,2})[Ag_8^+] \qquad (8B\text{-}1)$$

$$d[Ag_8O^+]/dt = k_{8B,1}[Ag_8^+] \qquad (8B\text{-}2)$$

$$d[Ag_6NO_2^+]/dt = k_{8B,2}[Ag_8^+] \qquad (8B\text{-}3).$$

The pathways (8A) and (8B) represent that $Ag_8NO_2^+$ is formed via Ag_8O^+ as an intermediate and that both Ag_8O^+ and $Ag_8NO_2^+$ are formed concurrently from Ag_8^+, respectively. The results of the curve fitting are shown by solid lines in Figs. 3a and 3b

for (8A) and (8B), respectively. The pseudo-first-order rate constants, $k_{8A,1}$ and $k_{8A,2}$, were 3.57 and 20.17 s^{-1}, respectively, in (8A), while $k_{8B,1}$ and $k_{8B,2}$ were 0.23 and 3.54 s^{-1}, respectively, in (8B). In contrast to Ag_6^+, the reaction pathway (8B) explains the temporal evolution of ion signals much better than (8A), suggesting that $Ag_8NO_2^+$ is not produced via an intermediate Ag_8O^+ but is formed from Ag_8^+ concurrently with Ag_8O^+. Direct formation of $Ag_8NO_2^+$ from Ag_8^+ should occur via an intermediate ion–molecule complex, either $Ag_8(NO)_2^+$ or $Ag_8(NO)_3^+$, which are not discernible in Fig. 1f. Formation of $Ag_8NO_2^+$ via $Ag_8(NO)_2^+$ or $Ag_8(NO)_3^+$ is accompanied by release of a neutral N atom or a N_2O molecule, respectively. In view of a possible high energy barrier for N-atom release, it is speculated that the $Ag_8NO_2^+$ formation proceeds via disproportionation, i.e., three NO molecules are converted to NO_2 and N_2O.[71]

3.2.3. Ag_{15}^+. Ag_{15}^+ forms $Ag_{15}O(NO_2)_{m-1}^+$ and $Ag_{15}(NO_2)_m^+$ in a similar way as Ag_8^+. Figure 4 shows temporal evolution of ion signals in the reaction of Ag_{15}^+ measured at $P_{NO} = 1 \times 10^{-2}$ Pa, where the reactant, Ag_{15}^+, disappears exponentially with the storage time, while $Ag_{15}N_2O_4^+$, $Ag_{15}N_3O_6^+$, $Ag_{15}N_4O_8^+$, and $Ag_{15}N_6O_{12}^+$ are observed as major product ions along with $Ag_{15}NO_3^+$, $Ag_{15}N_2O_5^+$, $Ag_{15}N_3O_7^+$, and $Ag_{15}N_4O_9^+$ as minor product ions. The analysis of kinetics was carried out in the same way as in the case of Ag_6^+ based on two reaction pathways (15A) and (15B):

$$\begin{aligned} &Ag_{15}^+ \xrightarrow{9.57} Ag_{15}O^+ \xrightarrow{59.34} Ag_{15}NO_2^+ \xrightarrow{11.69} Ag_{15}NO_3^+ \xrightarrow{118.95} Ag_{15}N_2O_4^+ \xrightarrow{9.41} Ag_{15}N_2O_5^+ \\ &\xrightarrow{40.51} Ag_{15}N_3O_6^+ \xrightarrow{12.19} Ag_{15}N_3O_7^+ \xrightarrow{180.52} Ag_{15}N_4O_8^+ \xrightarrow{1.75} Ag_{15}N_4O_9^+ \xrightarrow{14.99} Ag_{15}N_6O_{12}^+ \end{aligned} \quad (15A)$$

$$\begin{array}{l} Ag_{15}^{+} \xrightarrow{0.86} Ag_{15}O^{+} \xrightarrow{7.91} Ag_{15}NO_3^{+} \xrightarrow{14.69} Ag_{15}N_2O_5^{+} \xrightarrow{2.88} Ag_{15}N_3O_7^{+} \xrightarrow{6.18} Ag_{15}N_4O_9^{+} \\ \quad\quad \xrightarrow{8.81} Ag_{15}NO_2^{+} \xrightarrow{10.39} Ag_{15}N_2O_4^{+} \xrightarrow{8.35} Ag_{15}N_3O_6^{+} \xrightarrow{11.47} Ag_{15}N_4O_8^{+} \xrightarrow{1.14} Ag_{15}N_6O_{12}^{+} \end{array} \quad (15B).$$

The pseudo-first-order rate constants of each reaction are given above each arrow in s^{-1}. The results of the curve fitting are shown by solid lines in Figs. 4a and 4b for (15A) and (15B), respectively. As in the case of Ag_8^+, the reaction pathway (15B) explains the temporal evolution of ion signals much better than (15A), suggesting that $Ag_{15}(NO_2)_m^+$ is formed concurrently with $Ag_{15}O(NO_2)_{m-1}^+$ from $Ag_{15}(NO_2)_{m-1}^+$; major product ions, i.e., $Ag_{15}N_2O_4^+$, $Ag_{15}N_3O_6^+$, $Ag_{15}N_4O_8^+$, and $Ag_{15}N_6O_{12}^+$, are formed successively from $Ag_{15}NO_2^+$, whereas minor product ions, i.e., $Ag_{15}NO_3^+$, $Ag_{15}N_2O_5^+$, $Ag_{15}N_3O_7^+$, and $Ag_{15}N_4O_9^+$, are formed successively from $Ag_{15}O^+$. The addition of NO_2 might occur via an ion–molecule complex, $Ag_n(NO_2)_{m-1}(NO)_3^+$, accompanied by release of a neutral N_2O molecule by disproportionation as in the case of Ag_8^+. This pathway for NO_2 formation is different from that on a silver surface.[19] It is speculated that disproportionation is encouraged because three NO molecules are adsorbed closely with each other in a limited area on a cluster.

3.2.4. Other Sizes. The kinetics measurements and analyses were extended to n = 4–15 except for inert n = 3 and 5. The temporal evolution of ion signals for n = 4, 7, and 9–14 are shown in Figs. S1–S8 of the Supporting Information, respectively. In each figure, solid lines present fitting curves to pseudo-first-order rate equations based on the pathways below each panel. The pseudo-first-order rate constants of each step of reactions are given above each arrow in s^{-1}. All the panels (a) represent a pathway that $Ag_n(NO_2)_m^+$ is formed via $Ag_nO(NO_2)_{m-1}^+$ as an intermediate; the panels (b) assume that $Ag_nO(NO_2)_{m-1}^+$ and $Ag_n(NO_2)_m^+$ are formed concurrently from $Ag_n(NO_2)_{m-1}^+$.

For n = 4 and 9 in Figs. S1 and S3, the best fit was obtained for a pathway that Ag_nO^+ acts as an intermediate for $Ag_nNO_2^+$ as in the case of n = 6. For n = 4 (Fig. S1), Ag_4O^+ appears to be produced first, being followed by formation of $Ag_4NO_2^+$, while Ag_3^+ exhibits an exponential rise to dominate the product ions. The better fits in Fig. S1a rather than in Fig. S1b suggest that $Ag_4NO_2^+$ is formed via Ag_4O^+. For n = 9, $Ag_8NO_2^+$ as well as $Ag_9NO_2^+$ was produced via Ag_9O^+ as shown in Fig. S3. The results for n = 4, 6, and 9 are analogous to the reaction of NO reported for silver surfaces, where adsorption of two NO molecules on a silver surface produces N_2O and O at 75–100 K, and further reaction with another NO molecule produces NO_2.[19] In the present study of gas-phase clusters, $Ag_nO(NO_2)_{m-1}^+$ might be produced from an ion–molecule complex, $Ag_n(NO_2)_{m-1}(NO)_2^+$, which is not discernible in the mass spectra, and further reaction of $Ag_nO(NO_2)_{m-1}^+$ with another NO molecule produces $Ag_n(NO_2)_m^+$.

On the other hand, n = 7 and 10–12 are similar to n = 8 and 15, suggesting that $Ag_nNO_2^+$ is formed concurrently with Ag_nO^+, not via Ag_nO^+ intermediate. As for n =7 (Fig. S2), $Ag_7NO_2^+$ is formed from Ag_7^+ first. For further reaction, $Ag_7NO_3^+$ does not act as an intermediate for $Ag_7N_2O_4^+$, but $Ag_7NO_3^+$ and $Ag_7N_2O_4^+$ are concurrently formed from $Ag_7NO_2^+$. For n = 10 (Fig. S4), $Ag_{10}O^+$ and $Ag_{10}NO_2^+$ as well as Ag_9^+ and $Ag_9NO_2^+$ are concurrently formed from Ag_{10}^+. In the reaction of n = 12 (Fig. S6), $Ag_{12}O^+$ and $Ag_{12}NO_2^+$ are concurrently formed from Ag_{12}^+ in the first step, which produce $Ag_{12}NO_3^+$ and $Ag_{12}N_2O_4^+$, respectively, by further reaction with NO. $Ag_{12}N_2O_4^+$ further reacts with NO to produce $Ag_{12}N_3O_6^+$, where $Ag_{12}N_2O_5^+$ acts as an intermediate; this step is similar to the case of n = 4, 6, and 9.

Note that both the reaction pathways well-explain the behaviors of kinetics of n = 13 and 14. For n = 14, fitting curves both in Figs. S8a and in S8b reproduce the temporal

evolution; it was not possible to determine whether $Ag_{14}(NO_2)_m^+$ with m = 2–5 are successively formed via $Ag_{14}O(NO_2)_{m-1}^+$ as shown in Fig. S8a or not. Similary, the temporal evolution of ion signals for n =13 was well reproduced by fitting curves both in Figs. S7a and in S7b.

3.3. Size-Dependent Reactivity. Finally, the overall reaction rate coefficient was evaluated for each size of Ag_n^+ to show size-dependent reactivity; the extinction rate constants of the reactant cluster was divided by the number density of NO in the ion trap under the assumption that the elementary reaction is the first order for NO. Reaction rate coefficients thus obtained are plotted in Fig. 5 along with reaction rate coefficients against O_2 previously measured.[67] Note that the reactivity of Ag_3^+ and Ag_5^+ is so low that no product ion was observed in the present measurement, which is also the case for Ag_5^+, Ag_7^+, and Ag_9^+ reacting with O_2. In general, reactivity toward NO was found to be about three orders of magnitude higher, except for n = 3 and 5, than toward O_2. The size dependence shows odd−even alternation in common. The higher reactivity for even n is explained by higher adsorption energies of even-sized Ag_n^+ possessing an odd number of valence electrons as reported by theoretical studies.[39,40] The odd−even alternation is similar to that reported by a previous experimental study;[43] the magnitude of the oscillation is different at several sizes probably because of several adjustable conditions in the experiment such as temperature, reaction time, and flow rate of the NO gas.

4. CONCLUSIONS

We have performed kinetics measurement of the reaction of nitric oxide molecules on size-selected silver cluster cations, Ag_n^+ (n = 3–18), stored in an ion trap. The kinetics data were analyzed by fitting to rate equations to find the most probable reaction pathways

by examining various possible pathways; pseudo-first-order rate constants of each step of elementary reactions are thus obtained. Two reaction mechanisms were found for formation of major reaction products, i.e., $Ag_nO(NO_2)_{m-1}^+$ and $Ag_n(NO_2)_m^+$:

(1) Two NO molecules form neutral N_2O and Ag_nO^+, which further reacts with another NO molecule to produce $Ag_nNO_2^+$; $Ag_n(NO_2)_m^+$ is thus successively formed via an intermediate, $Ag_nO(NO_2)_{m-1}^+$. This reaction mechanism observed for n = 4, 6, and 9 is just analogous to that reported for bulk silver surfaces.

(2) Ag_nO^+ and $Ag_nNO_2^+$ are formed concurrently from Ag_n^+ exposed to NO molecules. The direct formation of the NO_2 adduct from Ag_n^+ implies NO disproportionation, i.e., three NO molecules are converted to NO_2 and N_2O via $Ag_n^+(NO)_3$ complex. These product ions, Ag_nO^+ and $Ag_nNO_2^+$, showed successive addition of NO_2 to produce $Ag_nO(NO_2)_{m-1}^+$ and $Ag_n(NO_2)_m^+$, respectively. These reaction channels were found at least for n = 7, 8, 10, 11, 12, and 15.

The overall reaction coefficient exhibited odd−even alternation, manifesting exceptionally inert n = 3 and 5 as well. The higher reactivity for even n, possessing an odd number of valence electrons, is consistent with higher adsorption energies of NO on even-sized Ag_n^+ as previously reported by theoretical studies.

ASSOCIATED CONTENT

Supporting Information

The Supporting Information is available free of charge on the ACS Publications website at DOI: xxx. Reaction kinetics of Ag_n^+ with NO for n = 4, 7, and 9–14.

AUTHOR INFORMATION

Corresponding Authors

* (M.A.) E-mail: arakawa@chem.kyushu-univ.jp

* (A.T.) E-mail: terasaki@chem.kyushu-univ.jp

Notes

The authors declare no competing financial interest.

ACKNOWLEDGMENTS

The present study was supported by Grants-in-Aid for Scientific Research (A) (JP18H03901) and for Scientific Research (C) (JP19K05185) from the Japan Society for Promotion of Science (JSPS), and for Scientific Research on Innovative Areas (JP17H06456) from the Ministry of Education, Culture, Sports, Science and Technology (MEXT). The computations were mainly performed using a computing system at the Research Institute for Information Technology, Kyushu University.

REFERENCES

(1) Ignarro, L. J.; Buga, G. M.; Wood, K. S.; Byrns, R. E.; Chaudhuri, G. Endothelium-Derived Relaxing Factor Produced and Released from Artery and Vein is Nitric Oxide. *Proc. Natl. Acad. Sci.* **1987**, *84*, 9265–9269.

(2) Hopper, R. A.; Garthwaite, H. Tonic and Phasic Nitric Oxide Signals in Hippocampal Long-Term Potentiation. *J. Neurosci.* **2006**, *26*, 11513–11521.

(3) Pârvulescu, V. I.; Grange, P.; Delmon, B. Catalytic Removal of NO. *Catal. Today* **1998**, *46*, 233–316.

(4) Hu, Y.; Griffiths, K.; Norton, P. R. Surface Science Studies of Selective Catalytic Reduction of NO: Progress in the Last Ten Years. *Surf. Sci.* **2009**, *603*, 1740–1750.

(5) Sotokawa, S. Enhancing the NO/C_3H_8/O_2 Reaction by Using H_2 over Ag/Al_2O_3 Catalysts under Lean-Exhaust Conditions. *Chem. Lett.* **2000**, *29*, 294–295.

(6) Shimizu, K.; Shibata, J.; Satsuma, A.; Hattori, T. Mechanistic Causes of the Hydrocarbon Effect on the Activity of Ag–Al_2O_3 Catalyst for the Selective Reduction of NO. *Phys. Chem. Chem. Phys.* **2001**, *3*, 880–884.

(7) Richter, M.; Bentrup, U.; Eckelt, R.; Schneider, M.; Pohl, M.-M.; Fricke, R. The Effect of Hydrogen on the Selective Catalytic Reduction of NO in Excess Oxygen over Ag/Al_2O_3. *Appl. Catal., B* **2004**, *51*, 261–274.

(8) He, H.; Yu, Y. Selective Catalytic Reduction of NO_x over Ag/Al_2O_3 Catalyst: from Reaction Mechanism to Diesel Engine Test. *Catal. Today* **2005**, *100*, 37–41.

(9) Kannisto, H.; Ingelsten, H. H.; Skoglundh, M. Ag–Al_2O_3 Catalysts for Lean NO_x Reduction—Influence of Preparation Method and Reductant. *J. Mol. Cata. A: Chem.* **2009**, *302*, 86–96.

(10) Kim, H. H.; Watanabe, K.; Menzel, D.; Freund, H.-J. Comparative Study of Thermal and Photo-Induced Reactions of NO on Particulate and Flat Silver Surfaces. *Surf. Sci.* **2012**, *606*, 1142–1151.

(11) Marbrow, R. A.; Lambert, R. M. Chemisorption and Surface Reactivity of Nitric Oxide on Clean and Sodium-Doped Ag(110). *Surf. Sci.* **1976**, *61*, 317–328.

(12) Behm, R. J.; Brundle, C. R. Summary Abstract: Decomposition of NO on Ag(111) at Low Temperatures. *J. Vac. Sci. Technol. A* **1984**, *2*, 1040.

(13) Nelin, C. J.; Bagus, P. S.; Behm, J.; Brundle, C. R. Core Level Photoemission of the NO Dimer: Theory and Experimental Realization for NO/Ag(111). *Surf. Sci.* **1984**, *105*, 58–63.

(14) Edamoto, K.; Maeshima, S.; Miyazaki, E.; Miyahara, T.; Kato, H. Angle-Resolved Photoemission Study of NO Chemisorption on Ag(111) Surface. *Surf. Sci.* **1988**, *204*, L739–L744.

(15) Jänsch, H. J.; Huang, C.; Ludviksson, A.; Rocker, G.; Redding, D. J.; Metiu, H.; Martin, R. M. Formation of N_2O from NO Adsorbed on Silver Layers on Ruthenium, Studied by MQS and TDS. *Surf. Sci.* **1989**, *214*, 377–395.

(16) So, S. K.; Franchy, R; Ho, W. The Adsorption and Reaction of NO on Ag(111) at 80 K. *J. Chem. Phys.* **1989**, *91*, 5701–5706.

(17) So, S. K.; Franchy, R; Ho, W. Photodesorption of NO from Ag(111) and Cu(111). *J. Chem. Phys.* **1991**, *95*, 1385–1399.

(18) Geuzebroek, F. H.; Wiskerke, A. E.; Tenner, M. G.; Kleyn, A. W.; Stolte, S.; Namiki, A. Rotational Excitation of Oriented Molecules as a Probe of Molecule-Surface Interaction. *J. Phys. Chem.* **1991**, *95*, 8409–8421.

(19) Ludviksson, A.; Huang, C.; Jänsch, H. J.; Martin, R. M. Isotopic Studies of the Reaction of NO on Silver Surfaces. *Surf. Sci.* **1993**, *284*, 328–336.

(20) Brown, W. A.; Gardner, P.; Jigato, M. P.; King, D. A. Characterization and Orientation of Adsorbed NO Dimers on Ag{111} at Low Temperatures. *J. Chem. Phys.* **1995**, *102*, 7277–7280.

(21) Brown, W. A.; Gardner, P.; King, D. A. Very Low Temperature Surface Reaction: N_2O Formation from NO Dimers at 70 to 90 K on Ag{111}. *J. Phys. Chem.* **1995**, *99*, 7065–7074.

(22) Rettner, C. T.; Auerbach, D. J.; Tully, J. C.; Kleyn, A. W. Chemical Dynamics at the Gas–Surface Interface. *J. Phys. Chem.* **1996**, *100*, 13021–13033.

(23) Carley, A. F.; Davies, P. R.; Roberts, M. W.; Santra, A. K.; Thomas, K. K. Coadsorption of Carbon Monoxide and Nitric Oxide at Ag(111): Evidence for a CO–NO Surface Complex. *Surf. Sci.* **1998**, *406*, L587–L591.

(24) Brown, W. A.; King, D. A. NO Chemisorption and Reactions on Metal Surfaces: A New Perspective. *J. Phys. Chem. B* **2000**, *104*, 2578–2595.

(25) Vondrak, T.; Burke, D. J.; Meech, S. R. The Dynamics and Origin of NO Photodesorbed from NO/Ag(111). *Chem. Phys. Lett.* **2000**, *327*, 137–142.

(26) King, D. A.; Carlisle, C. I. Direct Molecular Imaging of NO Monomers and Dimers and a Surface Reaction on Ag{111}. *J. Phys. Chem. B* **2001**, *105*, 3886–3893.

(27) Tenner, M. G.; Kuipers, E. W.; Kleyn, A. W.; Stolte, S. Classical Trajectory Study of the Interaction of Oriented NO and Ag(111). *Surf. Sci.* **1991**, *204*, 376–385.

(28) DePristo, A. E.; Alexande, M. H. Potential Energy Hypersurfaces for the Interaction of NO with the Ag(111) Surface. *J. Chem. Phys.* **1991**, *94*, 8454–8467.

(29) Gates, G. A.; Darling, G. R.; Holloway, S. A Theoretical Study of the Vibrational Excitation of NO/Ag(111). *J. Chem. Phys.* **1994**, *101*, 6281–6288.

(30) Jigato, M. P.; King, D. A.; Yoshimori, A. The Chemisorption of Spin Polarised NO on Ag{111}. *Chem. Phys. Lett.* **1999**, *300*, 639−644.

(31) Lang, S. M.; Bernhardt, T. M. Gas Phase Metal Cluster Model Systems for Heterogeneous Catalysis. *Phys. Chem. Chem. Phys.* **2012**, *14*, 9255−9269.

(32) Takagi, N.; Nakagaki, M.; Ishimura, K.; Fukuda, R.; Ehara, M.; Sakaki, S. Electronic Processes in NO Dimerization on Ag and Cu Clusters: DFT and MRMP2 Studies. *J. Comput. Chem.* **2019**, *40*, 181–190.

(33) Liu, Z.-P.; Jenkins, S. J.; King, D. A. Why Is Silver Catalytically Active for NO Reduction? A Unique Pathway via an Inverted $(NO)_2$ Dimer. *J. Am. Chem. Soc.* **2004**, *126*, 7336–7340.

(34) Kondo, Y.; Takahara, R.; Mohri, H.; Takagi, M.; Maeda, S.; Iwasa, T.; Taketsugu, T. Structural and Electronic Properties, Isomerization, and NO Dissociation Reactions on Au, Ag, Cu Clusters. *J. Comput. Chem., Jpn.* **2019,** *18*, 64–69.

(35) Citra, A.; Andrews, L. A. Spectroscopic and Theoretical Investigation of Charge Transfer Complexes between Silver and Nitric Oxide: Infrared Spectra and Density Functional Calculations of $AgNO^{+,0,-}$ and $Ag_x(NO)_y$ Clusters (x, y = 1, 2) in Solid Argon and Neon. *J. Phys. Chem. A* **2001**, *105*, 3042–3051.

(36) Matulis, V. E.; Ivashkevich, O. A. Comparative DFT Study of Electronic Structure and Geometry of Copper and Silver Clusters: Interaction with NO Molecule. *Comput. Mater. Sci.* **2006**, *35*, 268–271.

(37) Matulis, V. E.; Palagin, D. M.; Mazheika, A. S.; Ivashkevich, O. A. Theoretical Study of NO Adsorption on Neutral, Anionic and Cationic Ag_8 Clusters. *Comput. Theor. Chem.* **2011**, *963*, 422–426.

(38) Torbatian, Z.; Hashemifar, S. J.; Akbarzadeh, H. First-Principles Insights into Interaction of CO, NO, and HCN with Ag_8. *J. Chem. Phys.* **2014**, *140*, 084314.

(39) Grönbeck, H.; Hellman, A.; Gavrin, A. Structural, Energetic, and Vibrational Properties of NO_x Adsorption on Ag_n, n = 1–8. *J. Phys. Chem. A* **2007,** *111*, 6062–6067.

(40) Zhou, J.; Xiao, F.; Wang, W.-N.; Fan, K.-N. Theoretical Study of the Interaction of Nitric Oxide with Small Neutral and Charged Silver Clusters. *J. Mol. Struct.: THEOCHEM* **2007**, *818*, 51–55.

(41) Hagen, J.; Socaciu-Siebert, L. D.; Le Roux, J.; Popolan, D.; Vajda, S.; Bernhardt, T. M.; Wöste, L. Charge Transfer Initiated Nitroxyl Chemistry on Free Silver Clusters $Ag_{2–5}^-$: Size Effects and Magic Complexes. *Int. J. Mass Spectrom.* **2007**, *261*, 152–158.

(42) Baldansuren, A.; Eichel, R.-A.; Roduner, E. Nitrogen Oxide Reaction with Six-Atom Silver Clusters Supported on LTA Zeolite. *Phys. Chem. Chem. Phys.* **2009**, *11*, 6664–6675.

(43) Ma, J.; Cao, X.; Liu, H.; Yin, B.; Xing, X. The Adsorption and Activation of NO on Silver Clusters with Sizes up to One Nanometer: Interactions Dominated by Electron Transfer from Silver to NO. *Phys. Chem. Chem. Phys.* **2018**, *18*, 12819–12827.

(44) Klaassen, J. J.; Jacobson, D. B. Dissociative versus Molecular Chemisorption of Nitric Oxide on Small Bare Cationic Cobalt Clusters in the Gas Phase. *J. Am. Chem. Soc.* **1988**, *110*, 974–976.

(45) Hanmura, T.; Ichihashi, M.; Watanabe, Y.; Isomura, N.; Kondow, T. Reactions of Nitrogen Monoxide on Cobalt Cluster Ions: Reaction Enhancement by Introduction of Hydrogen. *J. Phys. Chem. A* **2007**, *111*, 422–428.

(46) Hanmura, T.; Ichihashi, M.; Okawa, R.; Kondow, T. Size-Dependent Reactivity of Cobalt Cluster Ions with Nitrogen Monoxide: Competition between Chemisorption and Decomposition of NO. *Int. J. Mass Spectrom.* **2009**, *280*, 184–189.

(47) Anderson, M. L.; Lacz, A.; Drewello, T.; Derrick, P. J.; Woodruff, D. P.; Mackenzie, S. R. The Chemistry of Nitrogen Oxides on Small Size-Selected Cobalt Clusters, Co_n^+. *J. Chem. Phys.* **2009**, *130*, 064305.

(48) Koyama, K.; Kudoh, S.; Miyajima, K.; Mafuné, F. Thermal Desorption Spectroscopy Study of the Adsorption and Reduction of NO by Cobalt Cluster Ions under Thermal Equilibrium Conditions at 300 K. *J. Phys. Chem. A* **2015**, *119*, 9573–9580.

(49) Vann, W. D.; Wagner, R. L.; Castleman, A. W., Jr. Gas-Phase Reactions of Nickel and Nickel-Rich Oxide Cluster Anions with Nitric Oxide. 2. The Addition of Nitric Oxide, Oxidation of Nickel Clusters, and the Formation of Nitrogen Oxide Anions. *J. Phys. Chem. A* **1998**, *102*, 8804–8811.

(50) Holmgren, L.; Andersson, M.; Rosén, A. NO on Copper Clusters. *Chem. Phys. Lett.* **1998**, *296*, 167–172.

(51) Hirabayashi, S.; Ichihashi, M. Reactions of Size-Selected Copper Cluster Cations and Anions with Nitric Oxide: Enhancement of Adsorption in Coadsorption with Oxygen. *J. Phys. Chem. A* **2014**, *118*, 1761–1768.

(52) Wu, Q.; Yang, S. Reactions of Niobium Cluster Ions $Nb_x^{\pm}$ (x = 2–16) with NO and NO_2. *Int. J. Mass Spectrom.* **1999**, *184*, 57–65.

(53) Ford, M. S.; Anderson, M. L.; Barrow, M. P.; Woodruff, D. P.; Drewello, T.; Derricka, P. J.; Mackenzie, S. R. Reactions of Nitric Oxide on Rh_6^+ Clusters: Abundant Chemistry and Evidence of Structural Isomers. *Phys. Chem. Chem. Phys.* **2005**, *7*, 975–980.

(54) Anderson, M. L.; Ford, M. S.; Derrick, P. J.; Drewello, T.; Woodruff, D. P.; Mackenzie, S. R. Nitric Oxide Decomposition on Small Rhodium Clusters, $Rh^{+/-}$. *J. Phys. Chem. A* **2006**, *110*, 10992–11000.

(55) Heinbuch, S.; Dong, F.; Rocca, J. J.; Bernstein, E. R. Experimental and Theoretical Studies of Reactions of Neutral Vanadium and Tantalum Oxide Clusters with NO and NH_3. *J. Chem. Phys.* **2010**, *133*, 174314.

(56) Hirabayashi, S.; Ichihashi, M. NO Decomposition Activated by Preadsorption of O_2 onto Copper Cluster Anions. *J. Phys. Chem. C* **2015**, *119*, 10850–10855.

(57) Nagata, T.; Miyajima, K.; Mafuné, F. Oxidation of Nitric Oxide on Gas-Phase Cerium Oxide Clusters via Reactant Adsorption and Product Desorption Processes. *J. Phys. Chem. A* **2015**, *119*, 10255–10263.

(58) Hirabayashi, S.; Ichihashi, M. Stability of Aluminum-Doped Copper Cluster Cations and Their Reactivity toward NO and O_2. *J. Phys. Chem. A* **2015**, *119*, 8557–8564.

(59) Haq, A.; Carew, A.; Raval, R. Nitric Oxide Reduction by Cu Nanoclusters Supported on Thin Al_2O_3 Films. *J. Catal.* **2004**, *221*, 204–212.

(60) Fielicke, A.; von Helden, G.; Meijer, G.; Simard, B.; Rayner, D. M. Direct Observation of Size Dependent Activation of NO on Gold Clusters. *Phys. Chem. Chem. Phys.* **2005**, *7*, 3906–3909.

(61) Yamaguchi, M; Kudoh, S.; Miyajima, K.; Lushchikoca, O. V.; Bakker, J. M.; Mafuné, F. Tuning the Dissociative Action of Cationic Rh Clusters Toward NO by Substituting a Single Ta Atom. *J. Phys. Chem. C* **2019**, *123*, 3476–3481.

(62) Gutsev, G. L.; Mochena, M. D.; Johnson, E.; Bauschlicher, C. W. Dissociative and Associative Attachment of NO to Iron Clusters. *J. Chem. Phys.* **2006**, *125*, 194312.

(63) Dutta, A.; Mondal, P. A Density Functional Study on the Electronic Structure, Nature of Bonding and Reactivity of NO Adsorbing $Rh_n^{0/\pm}$ (n = 2–8) Clusters. *New J. Chem.* **2018**, *42*, 1121–1132.

(64) Lacaze-Dufaurea, C.; Roquesb, J.; Mijoulea, C.; Siciliac, E.; Russoc, N.; Alexievd, V.; Mineva, T. A DFT Study of the NO Adsorption on Pd_n (n = 1–4) Clusters. *J. Mol. Catal. A: Chem.* **2011**, *341*, 28–34.

(65) Ding, X.; Li, Z.; Yang, J.; Hou, J. G.; Zhu, Q. Theoretical Study of Nitric Oxide Adsorption on Au Clusters. *J. Chem. Phys.* **2004**, *121*, 2558–2562.

(66) Teng, Y.-L.; Kohyama, M.; Haruta, M.; Xu, Q. Infrared Spectroscopic and Theoretical Studies on the Formation of Au_2NO^- and Au_nNO (n = 2–5) in Solid Argon. *J. Chem. Phys.* **2009**, *130*, 134511.

(67) Sarugaku, S.; Arakawa, M.; Kawano, T.; Terasaki, A. Electronic and Geometric Effects on Chemical Reactivity of 3d-Transition-Metal-Doped Silver Cluster Cations toward Oxygen Molecules. *J Phys. Chem. C* **2019**, 123, 25890–25897.

(68) Ito, T.; Egashira, K.; Tsukiyama, K.; Terasaki, A. Oxidation Processes of Chromium Dimer and Trimer Cations in an Ion Trap. *Chem. Phys. Lett.* **2012**, *538*, 19–23.

(69) Guo, B. C.; Kerns, K. P.; Castleman, A. W., Jr. Chemistry and Kinetics of Size-Selected Cobalt Cluster Cations at Thermal Energies. 2. Reactions with Oxygen. *J. Phys. Chem.* **1992**, *96*, 6931–6937.

(70) Handa, T.; Horio, T.; Arakawa, M.; Terasaki, A. Improvement of Reflectron Time-of-Flight Mass Spectrometer for Better Convergence of Ion Beam. *Int. J. Mass Spectrom.* **2020**, *451*, 116311.

(71) Ford, P. C.; Lorkovic, I. M. Mechanistic Aspects of the Reactions of Nitric Oxide with Transition-Metal Complexes. *Chem. Rev.* **2002**, *102*, 993−1018.

FIGURE CAPTIONS

Figure 1. Mass spectra of product ions upon reaction of Ag_n^+ with NO molecules for n = 3–18 in panels (a)–(p), respectively. The partial pressure of NO, P_{NO}, and storage time, t, are given in each panel.

Figure 2. Reaction kinetics of Ag_6^+ with NO. The ion signals of the reactant and products are plotted as a function of storage time; Ag_6^+ (closed circles), Ag_6O^+ (closed triangles), $Ag_6NO_2^+$ (closed squares), and Ag_5^+ (open diamonds). The partial pressure of NO was estimated to be about 3×10^{-3} Pa in the ion trap. Solid lines in panels (a) and (b) are fitting curves to pseudo-first-order rate equations based on reaction pathway (6A) and (6B), respectively. The best fit was obtained for (a).

Figure 3. Reaction kinetics of Ag_8^+ with NO. The ion signals of the reactant and products are plotted as a function of storage time; Ag_8^+ (closed circles), Ag_8O^+ (closed triangles), and $Ag_8NO_2^+$ (closed squares). The partial pressure of NO was estimated to be about 6×10^{-3} Pa in the ion trap. Solid lines in panels (a) and (b) are fitting curves to pseudo-first-order rate equations based on reaction pathway (8A) and (8B), respectively. The best fit was obtained for (b).

Figure 4. Reaction kinetics of Ag_{15}^+ with NO. Minor products are displayed in a magnified scale in (a′) and (b′). The ion signals of the reactant and products are plotted as a function of storage time; Ag_{15}^+ (closed circles), $Ag_{15}O^+$ (open squares), $Ag_{15}NO_2^+$ (closed squares), $Ag_{15}NO_3^+$ (open diamonds), $Ag_{15}N_2O_4^+$ (closed diamonds), $Ag_{15}N_2O_5^+$ (open triangles), $Ag_{15}N_3O_6^+$ (closed triangles), $Ag_{15}N_3O_7^+$ (open inversed triangles),

$Ag_{15}N_4O_8^+$ (closed inversed triangles), $Ag_{15}N_4O_9^+$ (open rhombus), and $Ag_{15}N_6O_{12}^+$ (closed rhombus). The partial pressure of NO was estimated to be about 1×10^{-2} Pa in the ion trap. Solid lines are fitting curves to pseudo-first-order rate equations based on the reaction pathway shown below each panel. The pseudo-first-order rate constants of each reaction are given above each arrow in s^{-1}. The best fit was obtained for (b); panel (a and a′) does not reproduce the behaviors of behaviors of $Ag_{15}N_3O_6^+$ and minor product ions.

Figure 5. Reaction rate coefficients of Ag_n^+ reacting with NO as a function of cluster size (closed circle). The rate coefficients with O_2 are superimposed in gray (closed square). The value $<10^{-16}$ indicates that no product ion was observed in the present measurement. Error bars indicate a systematic error of 30% due to the uncertainty in the partial pressure of NO in the reaction cell.

FIGURES

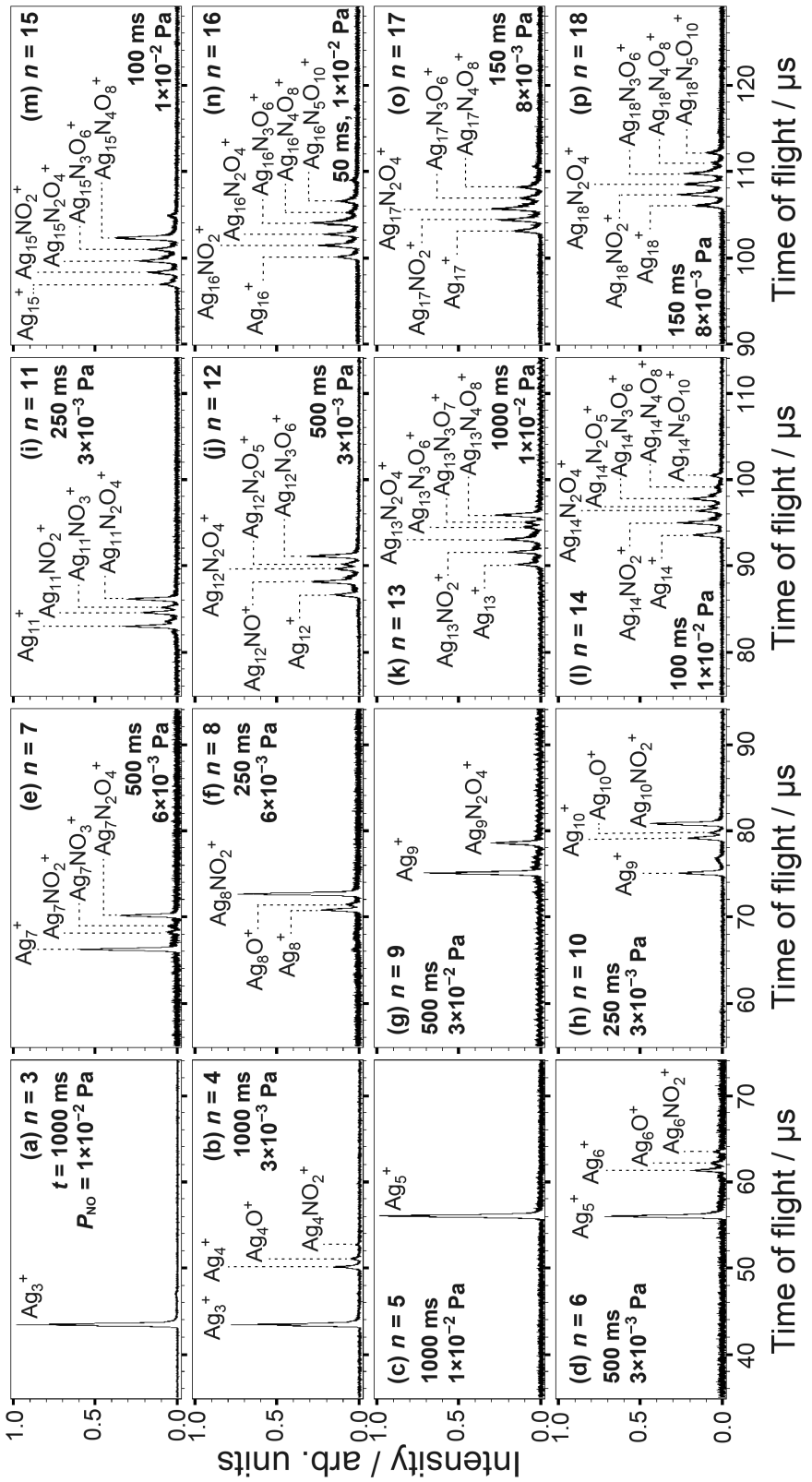

Figure 1. Arakawa et al.

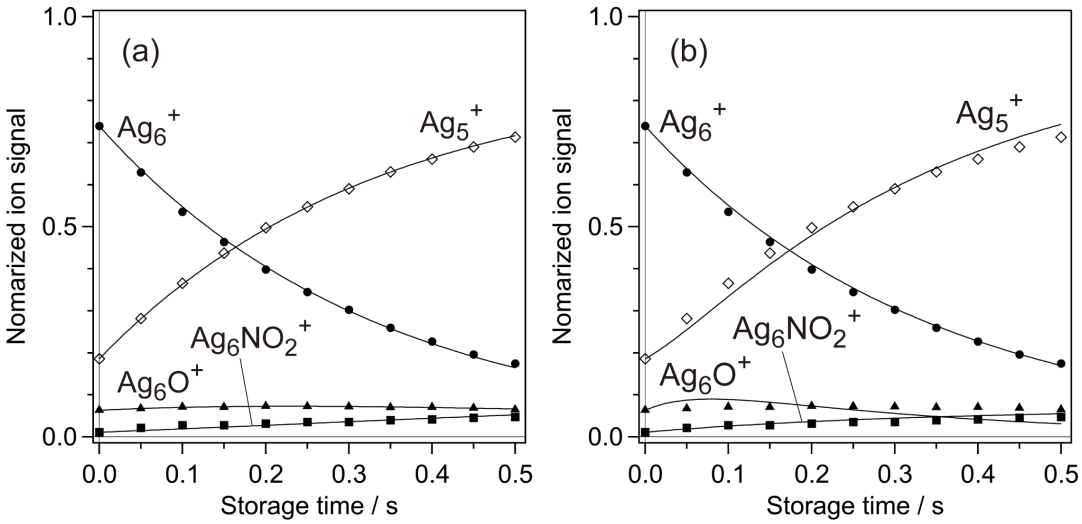

Figure 2. Arakawa et al.

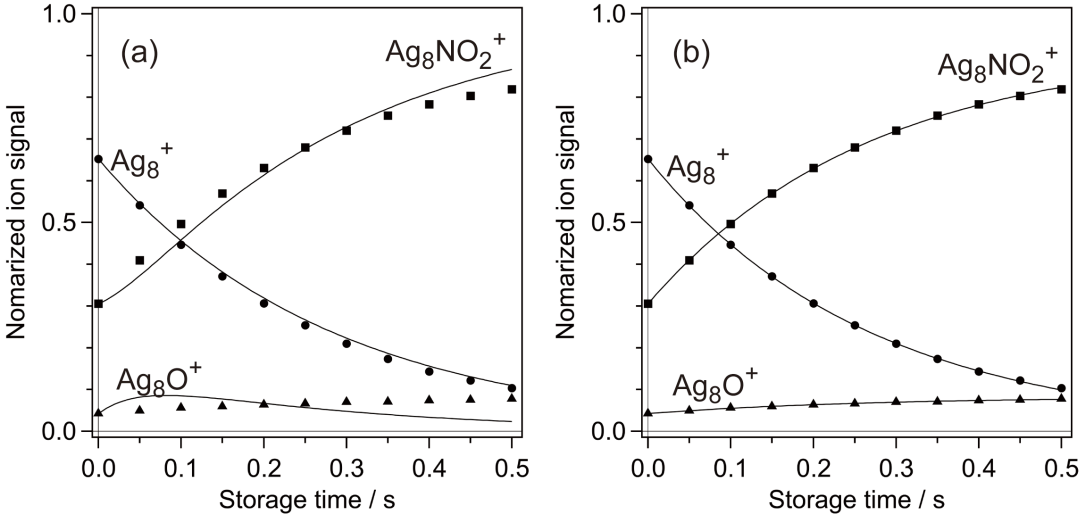

Figure 3. Arakawa et al.

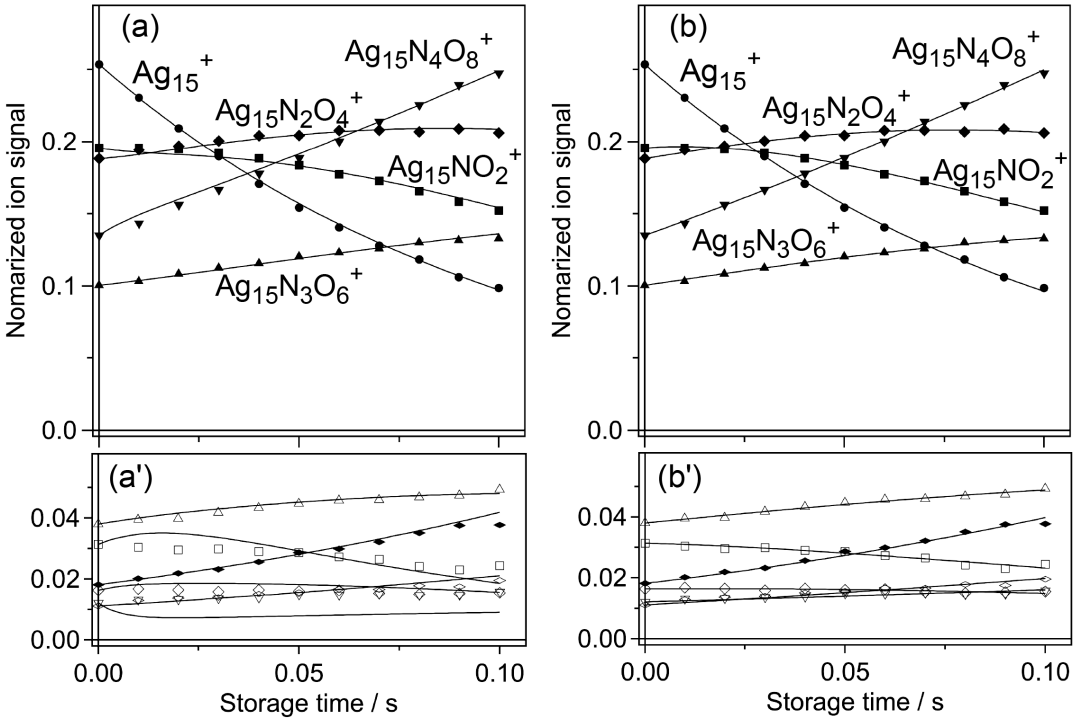

Figure 4. Arakawa et al.

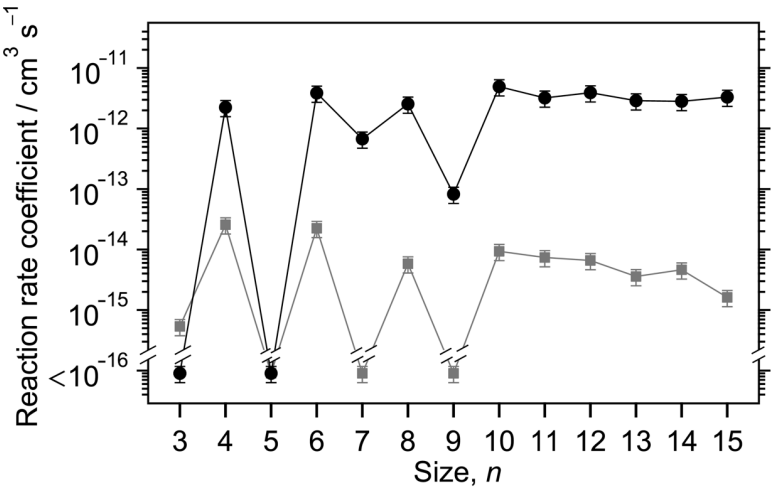

Figure 5. Arakawa et al.

Table of Content Artwork